Unclassified
SECURITY CLASSIFICATION OF THIS PAGE

REPORT DOCUMENTATION PAGE

Form Approved
OMB No. 0704-0188

1a. REPORT SECURITY CLASSIFICATION Unclassified	1b. RESTRICTIVE MARKINGS None
2a. SECURITY CLASSIFICATION AUTHORITY	3. DISTRIBUTION/AVAILABILITY OF REPORT Approved for public release; Distribution is unlimited.
2b. DECLASSIFICATION/DOWNGRADING SCHEDULE	
4. PERFORMING ORGANIZATION REPORT NUMBER(S) JA 221:088:88	5. MONITORING ORGANIZATION REPORT NUMBER(S) JA 221:088:88
6a. NAME OF PERFORMING ORGANIZATION Naval Ocean Research and Development Activity 6b. OFFICE SYMBOL (If applicable) 221	7a. NAME OF MONITORING ORGANIZATION Director, Ocean Acoustics and Technology Directorate
6c. ADDRESS (City, State, and ZIP Code) Stennis Space Center, MS 39529-5004	7b. ADDRESS (City, State, and ZIP Code) Stennis Space Center, MS 39529-5004
8a. NAME OF FUNDING/SPONSORING ORGANIZATION Naval Ocean Research and Development Activity 8b. OFFICE SYMBOL (If applicable) 221	9. PROCUREMENT INSTRUMENT IDENTIFICATION NUMBER
8c. ADDRESS (City, State, and ZIP Code) Stennis Space Center, MS 39529-5004	10. SOURCE OF FUNDING NUMBERS PROGRAM ELEMENT NO. 61153N; PROJECT NO. 03205; TASK NO. 330; WORK UNIT ACCESSION NO. 12219B

11. TITLE (Include Security Classification)
A nearfield asymptotic analysis for underwater acoustics

12. PERSONAL AUTHOR(S)
Michael D. Collins

13a. TYPE OF REPORT	13b. TIME COVERED	14. DATE OF REPORT (Year, Month, Day)	15. PAGE COUNT
Journal Article	FROM _____ TO _____	89, March	8

16. SUPPLEMENTARY NOTATION

17. COSATI CODES			18. SUBJECT TERMS (Continue on reverse if necessary and identify by block number)
FIELD	GROUP	SUB-GROUP	matched asymptotics; nearfield, Gaussian PE starter, TDPE, ray tracing

19. ABSTRACT (Continue on reverse if necessary and identify by block number)

The method of stationary phase is used to show that the homogeneous half-space field projects properly onto the normal modes near a point source. The half-space field is useful for initializing the parabolic equation (PE) in both the time domain and the frequency domain and in both two and three spatial dimensions. It si shown to be more accurate for wide-angle propagation than the Gaussian PE starter. A Gaussian time-doamin PE starter is derived and compared with the half-space starter. Application of the approach to scattering problems is discussed. The half-space field is the inner solution of a matched asymptotics solution. A simple approach for speeding up PE calculations and an efficient ray-tracing model for source localization are motivated by the matching.

20. DISTRIBUTION/AVAILABILITY OF ABSTRACT ☐ UNCLASSIFIED/UNLIMITED ☒ SAME AS RPT. ☐ DTIC USERS	21. ABSTRACT SECURITY CLASSIFICATION Unclassified
22a. NAME OF RESPONSIBLE INDIVIDUAL Mike Collins	22b. TELEPHONE (Include Area Code) 601 688-5853 22c. OFFICE SYMBOL 221

DD Form 1473, JUN 86 *Previous editions are obsolete.*

SECURITY CLASSIFICATION OF THIS PAGE
Unclassified

A nearfield asymptotic analysis for underwater acoustics

Michael D. Collins
Naval Ocean Research and Development Activity, Stennis Space Center, Mississippi 39529

(Received 1 September 1988; accepted for publication 30 November 1988)

The method of stationary phase is used to show that the homogeneous half-space field projects properly onto the normal modes near a point source. The half-space field is useful for initializing the parabolic equation (PE) in both the time domain and the frequency domain and in both two and three spatial dimensions. It is shown to be more accurate for wide-angle propagation than the Gaussian PE starter. A Gaussian time-domain PE starter is derived and compared with the half-space starter. Application of the approach to scattering problems is discussed. The half-space field is the inner solution of a matched asymptotics solution. A simple approach for speeding up PE calculations and an efficient ray-tracing model for source localization are motivated by the matching.

PACS numbers: 43.30.Bp, 43.30.Dr

UCTION

The parabolic equation[1] (PE) method requires that the acoustic field be specified at some range. The Gaussian PE starter[1,2] and more accurate PE starters[3,4] have been used widely to initialize the PE. These approaches are sufficient for solving two-dimensional time-harmonic propagation problems, but they are difficult to apply to three-dimensional, time-domain, and scattering problems. In this article, we consider a PE starter that is accurate, easy to construct and understand physically, and useful for both frequency-domain and time-domain problems in both two and three spatial dimensions including scattering problems.

Refraction in the ocean is weak and thus can be neglected near a sound source for a fairly large distance. Reflections from the ocean bottom can also be neglected near the source because the reflection coefficient at normal incidence is small. Reflection from the ocean surface, however, cannot be neglected because total reflection is usually assumed at the ocean surface. Thus the homogeneous half-space field is a valid approximation near a sound source. Far from the source, both refraction and reflection from the ocean bottom must be accounted for. Thus the half-space field breaks down in the farfield, and a boundary layer[5] exists near the source.

We use the method of stationary phase[6] to show that the half-space field projects properly onto the normal modes near the source. Thus the half-space field can be used to replace a source condition with a boundary condition on a cylinder enclosing the source to obtain an accurate farfield solution. We compare the half-space starter and the Gaussian PE starter in both the frequency domain and the time domain. For deep-water problems, the boundary layer behavior motivates an approach for speeding up PE calculations as well as an efficient ray-tracing model.

I. THE NORMAL-MODE SOLUTION

A time-harmonic steady state is assumed, and the acoustic pressure p is factored as $p(\mathbf{x},t) = P(\mathbf{x})\exp(-i\omega t)$, where t is time, $\mathbf{x}$ is the Cartesian position vector, and ω is the circular frequency. The complex pressure P is assumed to satisfy the pressure release boundary condition $P = 0$ at the ocean surface, the outgoing radiation condition at infinity, and the reduced wave equation[7]

$$\rho\nabla\cdot[(1/\rho)\nabla P] + K^2 P = -4\pi\delta(\mathbf{x}-\mathbf{x}_0), \tag{1}$$

where the point $\mathbf{x}_0$ is the source location. The complex wavenumber $K = k(1+i\sigma\beta)$ is used to model sediment loss, where the wavenumber is $k = \omega/c$, $\sigma = (40\pi\log_{10}e)^{-1}$, β is the attenuation in decibels per wavelength (dB/λ), and c is the sound speed. The variable density term is due to Bergmann.[8]

Since the ocean is a waveguide, energy propagating from a source exhibits cylindrical spreading in the absence of azimuthal variation in the ocean. Thus it is often beneficial to solve Eq. (1) in cylindrical coordinates, with z being the depth below the ocean surface and r being the horizontal distance from a source at the depth z_0. Variations in both azimuth and range are assumed to be sufficiently weak so that the region near the source can be treated as stratified, which simplifies Eq. (1) to

$$\frac{\partial^2 P}{\partial z^2} - \frac{1}{\rho}\frac{d\rho}{dz}\frac{\partial P}{\partial z} + \frac{\partial^2 P}{\partial r^2} + \frac{1}{r}\frac{\partial P}{\partial r} + K^2 P = -\frac{2}{r}\delta(r)\delta(z-z_0). \tag{2}$$

The normal-mode solution[7] of Eq. (2), which is valid in the limit $kr \gg 1$ and $\sigma\beta \ll 1$, is

$$P(r,z) \sim \sqrt{\frac{2\pi i}{r}} \sum_{n=1}^{N} \phi_n(z_0)\phi_n(z)\frac{\exp[(ik_n - \gamma_n)r]}{\sqrt{k_n}}, \tag{3}$$

$$L\phi_n = \left(\frac{d^2}{dz^2} - \frac{1}{\rho}\frac{d\rho}{dz}\frac{d}{dz} + k^2\right)\phi_n = k_n^2\phi_n, \tag{4}$$

where $\phi_n(0) = \phi_n(\infty) = 0$, and N is the number of modes in the discrete spectrum of L. The normal modes satisfy $\langle\phi_m,\phi_n\rangle = \delta_{mn}$, where the inner product associated with L is defined by

$$\langle g,h\rangle = \int_0^\infty \frac{g(z)h(z)}{\rho(z)}\,dz. \tag{5}$$

The constants γ_n are defined by

 0001-4966/89/031107-08$00.80

$$\gamma_n = k_0 \sigma \langle \beta, \phi_n^2 \rangle, \tag{6}$$

where $k_0 = k(z_0)$. The vertical propagation angles α_n are defined by

$$k_n = k_0 \cos \alpha_n. \tag{7}$$

In the Appendix, we present a direct asymptotic derivation of Eq. (6), which has also been derived using the Rayleigh quotient.[7]

We do not consider frequencies less than ω_0, the frequency below which L does not have a discrete spectrum. For each frequency $\omega > \omega_0$, we define $A(\omega)$ to be the maximum of α_n over n. We define ϵ to be the maximum of $\tan^2 A(\omega)$ over ω. The discontinuity in sound speed at the ocean bottom $z = d(r)$ is relatively small. Thus energy propagation is limited to small vertical angles, and we assume that $\epsilon \ll 1$.

II. THE HOMOGENEOUS HALF-SPACE FIELD

Equation (2) is difficult to solve numerically near the source because P and the Laplacian are singular at $r = 0$. This problem can be handled by solving Eq. (2) asymptotically near the source for $r < r_0$. Any function that properly excites the normal modes can be used as a boundary condition at $r = r_0$ to replace the source condition at $r = 0$. In the high-frequency limit, it is necessary to accurately account only for the trapped rays that propagate within the angle A of the horizontal; and the homogeneous half-space field projects properly onto the normal modes at $r = r_0$ if trapped rays do not reflect from the ocean bottom and are not significantly affected by refraction in the ocean for $r < r_0$. This asymptotic solution breaks down for large r_0. Thus a boundary layer exists near $r = 0$, and the half-space solution is an inner solution. We will use the method of stationary phase to demonstrate the validity of the half-space solution and to show when it is valid.

In the homogeneous half-space with $\beta = 0$, the solution of Eq. (2) is

$$P_h(r,z) = \exp(ikd_-)/d_- - \exp(ikd_+)/d_+, \tag{8}$$

$$d_\pm^2 = r^2 + (z \pm z_0)^2. \tag{9}$$

Since a ray propagating with small vertical angle α remains in $z < d$ for small r, one would expect that

$$\langle P_h, \phi_n \rangle \sim \langle P, \phi_n \rangle. \tag{10}$$

Since $\beta(z) = 0$ for $z < d$ and $\phi_n(z)$ is evanescent for $z > d$, it follows from Eq. (6) that $k_n^{-1}\gamma_n \ll \sigma\beta \ll 1$. We assume $\gamma_n r \ll 1 \ll k_n r$, and the factor $\exp(-\gamma_n r)$ may be dropped in Eq. (3). We obtain

$$\langle P, \phi_n \rangle \sim \sqrt{\frac{2\pi i}{kr \cos \alpha_n}}\, \phi_n(z_0) \exp(ikr \cos \alpha_n). \tag{11}$$

We establish Eq. (10) for the case in which c is constant in the water column. Thus

$$\phi_n(z) = a_n \sin(kz \sin \alpha_n) \tag{12}$$

for $z < d$, where a_n is a normalization constant. Because $\phi_n(z)$ is evanescent for $z > d$,

$$\langle P_h, \phi_n \rangle \sim (a_n/2i)[I_+(r) - I_-(r) - J_+(r) + J_-(r)], \tag{13}$$

$$I_\pm(r) = \int_0^d \frac{\exp\{ik[\sqrt{r^2 + (z - z_0)^2} \pm z \sin \alpha_n]\}}{\sqrt{r^2 + (z - z_0)^2}}\, dz, \tag{14}$$

$$J_\pm(r) = \int_0^d \frac{\exp\{ik[\sqrt{r^2 + (z + z_0)^2} \pm z \sin \alpha_n]\}}{\sqrt{r^2 + (z + z_0)^2}}\, dz. \tag{15}$$

Since the first mode is essentially half of a cycle of a sinusoid for $z < d$, we deduce from Eq. (12) that $kd \sin \alpha_1 = O(1)$. This implies that $kd \gg 1$ because $\sin \alpha_1 \ll 1$. Thus I_+ and J_- may be evaluated by the method of stationary phase with the length scale taken to be d. First, we consider

$$I_- = \int_0^d B(z) \exp[ik\psi(z)]\, dz, \tag{16}$$

$$\psi = \sqrt{r^2 + (z - z_0)^2} - z \sin \alpha_n, \tag{17}$$

$$\psi' = \frac{z - z_0}{\sqrt{r^2 + (z - z_0)^2}} - \sin \alpha_n, \tag{18}$$

$$\psi'' = r^2[r^2 + (z - z_0)^2]^{-3/2}. \tag{19}$$

From Eq. (18), ψ' vanishes at $z_s = z_0 + r \tan \alpha_n$. This is a stationary point of I_- if $z_s < d$, which occurs if

$$r < r_n = (d - z_0) \cot \alpha_n. \tag{20}$$

This stationary point corresponds to the ray propagating downward at the angle α_n. At the stationary point,

$$B = r^{-1} \cos \alpha_n, \tag{21}$$

$$\psi = r \cos \alpha_n - z_0 \sin \alpha_n, \tag{22}$$

$$\psi'' = (r \cos^3 \alpha_n)^{-1}. \tag{23}$$

Thus we obtain

$$I_-(r) \sim \sqrt{2\pi i/kr \cos \alpha_n} \times \exp(ikr \cos \alpha_n - ikz_0 \sin \alpha_n). \tag{24}$$

A similar analysis for I_+ gives $z_s = z_0 - r \tan \alpha_n$. If $z_s > 0$, this is a stationary point of I_+. If $z_s < 0$, I_+ does not have a stationary point, and J_+ has the stationary point $-z_s = -z_0 + r \tan \alpha_n$. These stationary points correspond to the ray propagating upward at the angle α_n; $I_+(J_+)$ has the stationary point if the ray has not (has) reflected from the ocean surface. If $z_s = 0$, I_+ and J_+ share this stationary point. Here, J_- never has a stationary point. In each case, we find that

$$I_+(r) - J_+(r) + J_-(r) \sim \sqrt{2\pi i/kr \cos \alpha_n} \times \exp(ikr \cos \alpha_n + ikz_0 \sin \alpha_n), \tag{25}$$

$$\langle P_h, \phi_n \rangle \sim \sqrt{2\pi i/kr \cos \alpha_n} \times a_n \sin(kz_0 \sin \alpha_n) \exp(ikr \cos \alpha_n). \tag{26}$$

Thus P_h properly excites the normal modes.

The above analysis is easily modified to handle the case in which c varies in the water; however, several cases must be considered. If $\phi_n(z)$ is not evanescent near $z = z_0$, then α_n is

real, and the following expansion is valid for $z \sim z_0$:

$$\phi_n(z) \sim b_n \sin(k_0 z \sin \alpha_n + d_n) , \tag{27}$$

where b_n and d_n are constants with $0 \leq d_n < 2\pi$. The stationary phase analysis goes through similarly in this case. However, r must be chosen sufficiently small so that Eq. (27) is valid at the stationary points. If $\phi_n(z)$ is evanescent near $z = z_0$, it suffices to show that the projection of P_h onto ϕ_n is subdominant to the projection of P_h onto other modes; ϕ_n is not incorporated into the exponentials in Eqs. (14) and (15) in this case. A similar analysis results in

$$\langle P_h, \phi_n \rangle \sim \sqrt{2\pi i / kr}\, \phi_n(z_0) \exp(ikr). \tag{28}$$

Since $\phi_n(z_0) \ll 1, \langle P_h, \phi_n \rangle$ is subdominant. It is possible that Eq. (28) is not valid if the main contribution of one of the integrals does not come from a stationary point. However, the contribution is automatically subdominant in this case.

According to Eq. (20), r must be small enough so that a ray from the source propagating at the angle α_n does not intersect the sediment. In the geometrical optics limit, r_n is the range at which P_h breaks down for rays propagating with vertical angles $\alpha < \alpha_n$. For lower frequencies, one would expect P_h to break down for smaller r. The stationary phase approximation is valid if $\exp(ik\psi)$ oscillates rapidly away from the stationary point. This occurs if

$$k|\psi'| = k \left| \frac{z - z_0}{\sqrt{r^2 + (z - z_0)^2}} - \sin \alpha_n \right| \gg 1 \tag{29}$$

for $|z - z_s| = O(1)$. Since $\psi'(z) = O(\sin \alpha_n)$ or larger for $|z - z_s| = O(1)$, Eq. (29) holds for the case $k \sin \alpha_n \gg 1$.

For $k \sin \alpha_n = O(1)$, Eq. (29) is equivalent to

$$k|z - z_0| / \sqrt{r^2 + (z - z_0)^2} \gg 1. \tag{30}$$

Let $r = \kappa r_n = \kappa(d - z_0)\cot \alpha_n$, where

$$\kappa(d - z_0) \ll 1. \tag{31}$$

From Eq. (31), $|z_s - z_0| = \kappa|d - z_0| \ll 1$. We deduce that $|z - z_s| = O(1)$ is equivalent to $|z - z_0| = O(1)$, and the stationary phase approximation is valid if Eq. (30) holds for $|z - z_0| = O(1)$. For $r = O(1)$, Eq. (30) holds since $k \gg 1$. Due to the fact that $k \sin \alpha_n = O(1)$, Eq. (30) follows from Eq. (31) for $r \gg 1$. Thus the stationary phase evaluation of the integrals in Eqs. (14) and (15) is valid for $r \ll r_n$ if $d - z_0 = O(1)$ and for $r < r_n$ if $d - z_0 \ll 1$ or $k \sin \alpha_n \gg 1$.

III. APPLICATIONS

With the inner solution, it is possible to avoid the singular nature of Eq. (2) near $r = 0$. The source condition at $r = 0$ is replaced by the boundary condition $P(r_0, z) = P_h(r_0, z)$. There is an additional problem to be dealt with, however, before the outer problem can be solved numerically in the outer region $r > r_0$. The infinite spatial domain must be truncated. The outer solution of Eq. (2) replaces the boundary value problem with an initial value problem in range taking care of half of this problem. The problem is truncated in depth with the boundary condition $P(r, z_M) = 0$, where z_M is large. Since the sediment is lossy, only a negligible amount of energy can travel to the lower boundary and return to the water column. Thus only a small error is introduced by truncating the domain. The inner solution P_h does not satisfy the pressure release boundary condition at $z = z_M$, resulting in Gibbs' oscillations. However, the propagating modes in the truncated domain are evanescent for $z > d$. Thus the Gibbs' oscillations project onto nonpropagating modes and decay rapidly with r causing little error in the farfield.

The major benefit of the half-space field is that it can be applied to several problems. If azimuthal variations are assumed to be a weak perturbation, the half-space field can be applied to initialize the three-dimensional parabolic equation at $r = r_0$. For a pulsed source with the source function $f(t)$ of finite bandwidth, the homogeneous half-space field

$$p_h(r,z,t) = \frac{1}{d_-} f\left(t - \frac{d_-}{c_0}\right) - \frac{1}{d_+} f\left(t - \frac{d_+}{c_0}\right) \tag{32}$$

is a valid inner solution of the time-domain problem by the superposition principle since it is valid for each frequency composing the source. The source condition at $r = 0$ is replaced by the boundary condition $p(r_0, z, t) = p_h(r_0, z, t)$. This starter has been applied to initialize the time-domain parabolic equation[9] (TDPE) and the progressive wave equation[10] producing accurate results.

The inner solution can also be applied to simplify the waveguide scattering problem for a bounded object in $0 < z < d$. Previous work on this problem has not exploited asymptotic limits.[11,12] The total field P_t is defined to be the sum of the incident and scattered fields P_i and P_s, z_0 is assumed to be a parameter, and the solution of Eq. (2) is written as $P(r, z; z_0)$. The scattered field has the representation

$$P_s(\mathbf{x}) = \int\int \left(\frac{\partial G}{\partial n}(\mathbf{x}, \mathbf{x}_0) P_t(\mathbf{x}_0) - \frac{\partial P_t}{\partial n}(\mathbf{x}_0) G(\mathbf{x}, \mathbf{x}_0) \right) d\mathbf{x}_0, \tag{33}$$

where G is the waveguide Green's function defined by

$$G(\mathbf{x}, \mathbf{x}_0) = (1/4\pi) P\left[\sqrt{(x - x_0)^2 + (y - y_0)^2}, z; z_0\right] . \tag{34}$$

The integral is over the surface of the scatterer. Since G is the field due to a point source, and $\partial G / \partial n$ can be approximated by two point sources, P_s may be regarded as the field due to a collection of point sources on and near the surface of the scatterer. Thus the scatterer behaves like a collection of point sources, which suggests that a valid inner solution for the scattering problem consists of the solution of the scattering problem in the homogeneous half-space. This is a significant simplification of the waveguide scattering problem because useful methods for solving the half-space problem have been developed. An asymptotic analysis of the waveguide scattering problem is given in Ref. 13.

IV. COMPARISON WITH THE GAUSSIAN PE STARTER

There is an alternate method for dealing with the singular behavior near the source. From Eq. (3), it follows that $P \sim r^{-1/2} Q$ in the farfield, where

$$\frac{\partial^2 Q}{\partial z^2} - \frac{1}{\rho} \frac{d\rho}{dz} \frac{\partial Q}{\partial z} + \frac{\partial^2 Q}{\partial r^2} + k^2 Q = 0, \tag{35}$$

$$Q(0,z) = \sqrt{2\pi i} \sum_n \frac{\phi_n(z_0)\phi_n(z)}{\sqrt{k_n}} . \tag{36}$$

TABLE I. Data for the frequency-domain nearfield problem.

$z_0 = 50$ m	$\omega = 500\pi^{-1}$	$d = 100$ m
$c = 1500$ m/s	$c_b = 1590$ m/s	$\rho = 1$ g/cm^3
$\beta = 0$	$\rho_b = 1.2$ g/cm^3	$\beta_b = 0.5$ dB/λ
$r_0 = 50$ m		

TABLE III. Data for the time-domain nearfield problem.

$z_0 = 75$ m	$\nu = 150$ s^{-1}	$d = 200$ m
$c = 1500$ m/s	$c_b = 1600$ m/s	$\rho_w = 1$ g/cm^3
$\beta = 0$	$\rho_b = 1.5$ g/cm^3	$\beta_b = 0.5$ dB/λ
$r_0 = 50$ m	$w = 10$ m	

To avoid computing normal modes, the Gaussian PE starter

$$\Gamma(z,z_0;k_0) = \sqrt{\frac{ik_0}{2}}\left[\exp\left(\frac{-k_0^2(z-z_0)^2}{4}\right) - \exp\left(\frac{-k_0^2(z+z_0)^2}{4}\right)\right], \tag{37}$$

which approximates $D(z,z_0;k_0) = (2\pi i/k_0)^{1/2}[\delta(z-z_0) - \delta(z+z_0)]$, is used in place of Eq. (36) as an initial condition at $r = 0$. This is a valid approximation since $k_n \sim k_0$ and

$$\langle Q,\phi_n\rangle = \sqrt{2\pi i/k_n}\,\phi_n(z_0), \tag{38}$$

$$\langle D,\phi_n\rangle = \sqrt{2\pi i/k_0}\,\phi_n(z_0). \tag{39}$$

Since k_n diverges from k_0 as α_n increases, we see from Eqs. (26) and (39) that P_h excites the higher modes better than D, which should excite modes better than the approximation Γ. We illustrate this with an example for which data appear in Table I. The subscript w stands for water value. The subscript b stands for bottom value. Projections of P_h, D, and Γ onto the modes appear in Table II. We observe that the error in P_h is small and uniform in α_n, while the error in Γ increases with α_n and is larger than the error in D for all α_n.

A pulsed source function is decomposed as

$$f(t) = \int_{-\infty}^{\infty} F(\omega)\exp(-i\omega t)\,d\omega. \tag{40}$$

By superposition, $p \sim r^{-1/2}q$ in the farfield, where

$$\frac{\partial^2 q}{\partial z^2} - \frac{1}{\rho}\frac{d\rho}{dz}\frac{\partial q}{\partial z} + \frac{\partial^2 q}{\partial r^2} = \frac{1}{c^2}\frac{\partial^2 q}{\partial t^2}, \tag{41}$$

$$q(0,z,t) = \int_{-\infty}^{\infty} F(\omega)Q\left(0,z;\frac{\omega}{c_0}\right)\exp(-i\omega t)\,d\omega, \tag{42}$$

and $c_0 = c(z_0)$. We consider the source function $f(t) = \exp[-(\nu t)^2]$, for which

$$F(\omega) = (2\nu\sqrt{\pi})^{-1}\exp[-(\omega/2\nu)^2]. \tag{43}$$

TABLE II. Projections of P_h, Γ, and D onto modes.

k_n(m^{-1})	γ_n(m^{-1})	α_n(°)	$\frac{\langle P_h,\phi_n\rangle}{\langle P,\phi_n\rangle}$	$\frac{\langle \Gamma,\phi_n\rangle}{\langle P,\phi_n\rangle}$	$\frac{\langle D,\phi_n\rangle}{\langle P,\phi_n\rangle}$
1.04676	0.00000	1.65951	0.99907	0.99895	0.99979
1.04544	0.00002	3.31619	1.01666	0.99581	0.99916
1.04323	0.00004	4.96723	1.00280	0.99060	0.99812
1.04014	0.00007	6.60980	0.98127	0.98333	0.99667
1.03616	0.00012	8.24106	0.99439	0.97407	0.99482
1.03126	0.00017	9.85815	1.02109	0.96285	0.99259
1.02546	0.00024	11.45808	1.00875	0.94974	0.98999
1.01874	0.00033	13.03760	0.97815	0.93483	0.98703
1.01109	0.00046	14.59277	0.98854	0.91823	0.98374
1.00252	0.00068	16.11757	1.01759	0.90008	0.98015
0.99314	0.00126	17.59651	1.01015	0.88069	0.97632

Substituting D for Q in Eq. (42), we obtain

$$q(0,z,t) = \frac{1}{\nu}\sqrt{\frac{c_0}{2}}\,[\delta(z-z_0) - \delta(z+z_0)] \times \int_{-\infty}^{\infty}\left(\frac{i}{\omega}\right)^{1/2}\exp\left[-\left(\frac{\omega}{2\nu}\right)^2\right]\exp(-i\omega t)\,d\omega. \tag{44}$$

The delta function in Eq. (44) can be approximated by a Gaussian of width w:

$$\delta(z) \cong (w\sqrt{\pi})^{-1}\exp[-(z/w)^2]. \tag{45}$$

Substituting Eq. (45) in Eq. (44) and manipulating the integral, we obtain the Gaussian TDPE starter:

$$q(0,z,t) = \frac{1}{w\nu}\sqrt{\frac{2c_0}{\pi}} \times\left\{\exp\left[-\left(\frac{z-z_0}{w}\right)^2\right] - \exp\left[-\left(\frac{z+z_0}{w}\right)^2\right]\right\} \times\int_0^{\infty}\frac{1}{\sqrt{\omega}}\exp\left[-\left(\frac{\omega}{2\nu}\right)^2\right]\cos\left(\omega t - \frac{\pi}{4}\right)d\omega. \tag{46}$$

We consider the example described in Table III. The numerical solution of the TDPE requires that $q(r,z,t) \to 0$ rapidly as $t \to -\infty$ (see Ref. 9). We see from Fig. 1 that this condition holds. A sequence of contour plots generated using the TDPE with the Gaussian starter appears in Fig. 2. From the plots generated using the half-space starter, which appear in Fig. 3, we deduce that the Gaussian starter evolves properly. The accuracy of the Gaussian starter is illustrated quantitatively in Fig. 4. The error in the surface-reflected arrival near $t = 60$ ms, which propagates at roughly 15°, is on the order of 10%. We see from Table II that this error is of the appropriate magnitude.

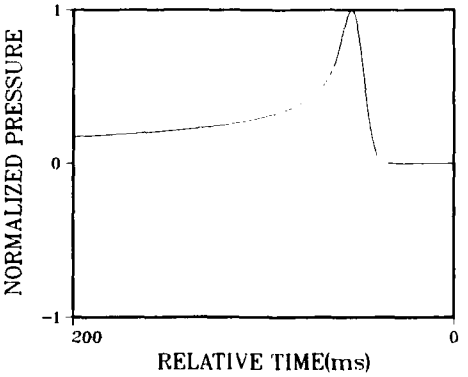

FIG. 1. The Gaussian TDPE starter at $z = 75$ m.

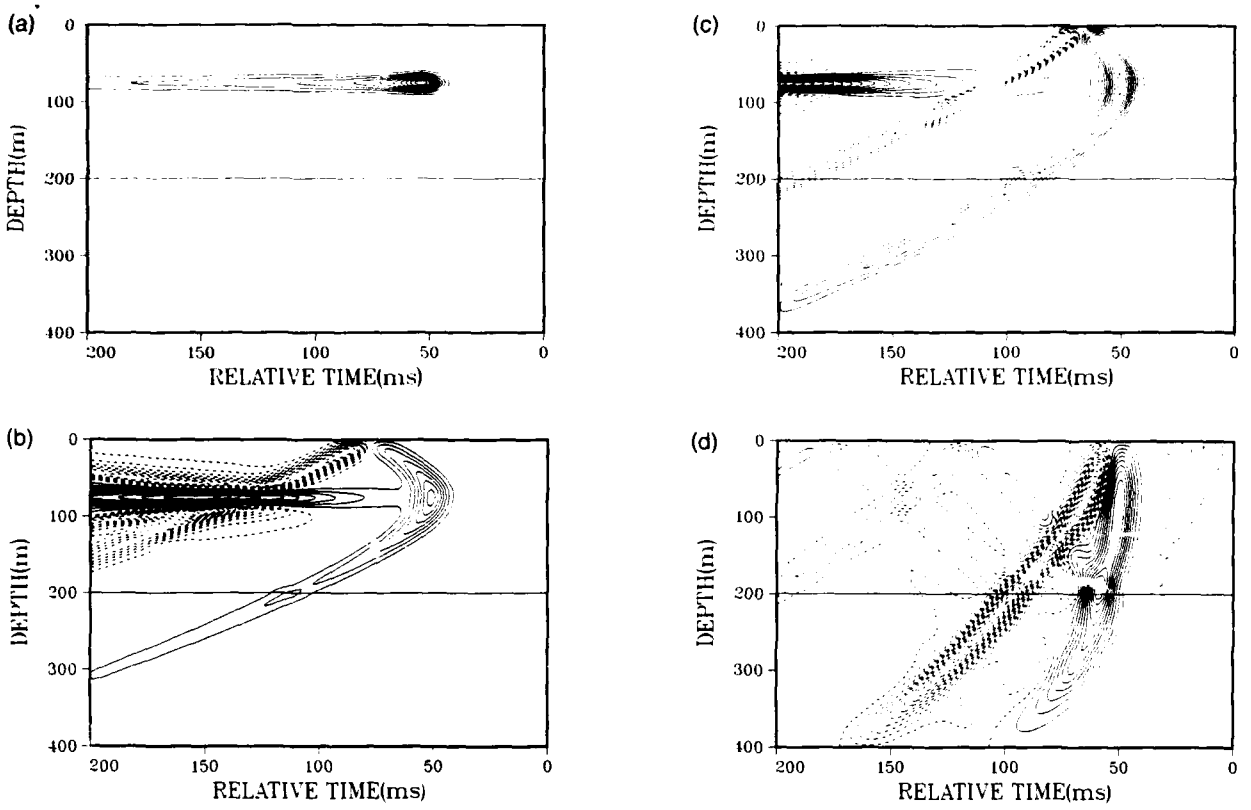

FIG. 2. TDPE solution generated with the Gaussian starter. The solid contours correspond to $p > 0$. The dashed contours correspond to $p < 0$. (a) $r = 0$, (b) $r = 50$ m, (c) $r = 100$ m, (d) $r = 500$ m.

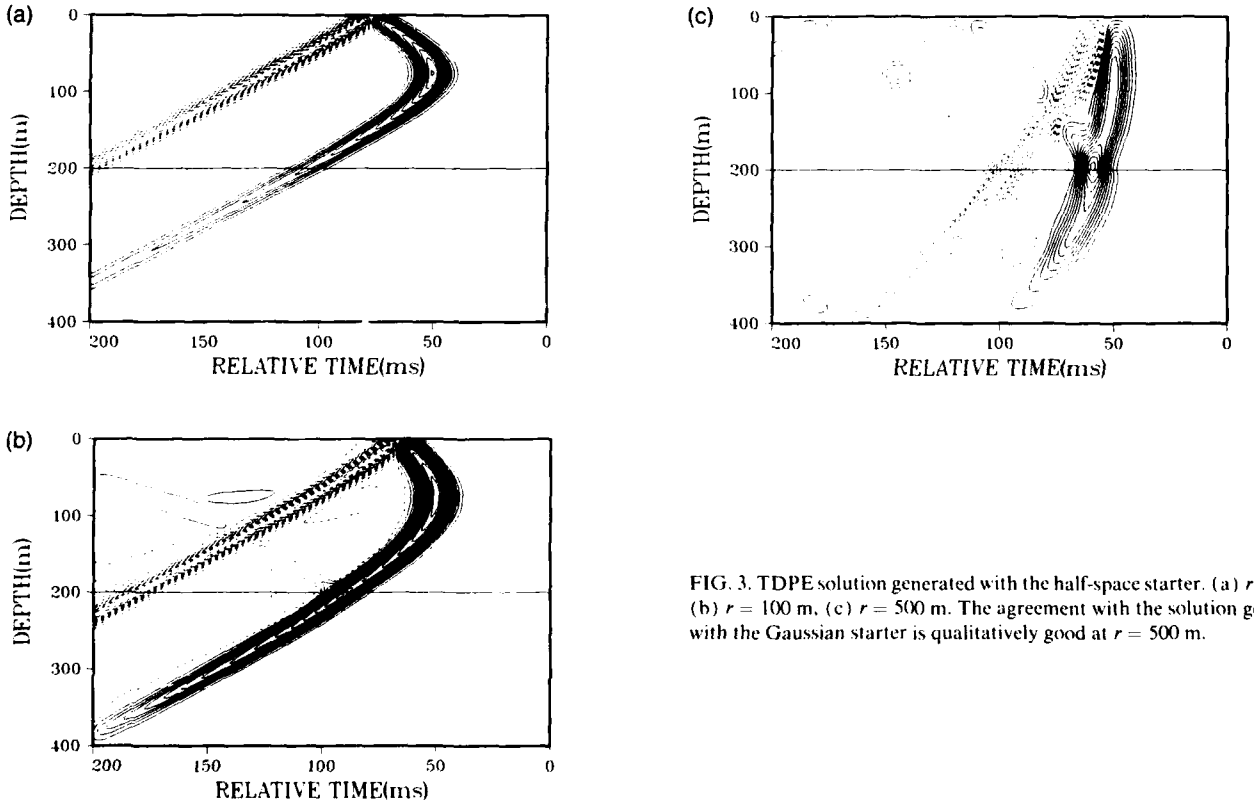

FIG. 3. TDPE solution generated with the half-space starter. (a) $r = 50$ m, (b) $r = 100$ m, (c) $r = 500$ m. The agreement with the solution generated with the Gaussian starter is qualitatively good at $r = 500$ m.

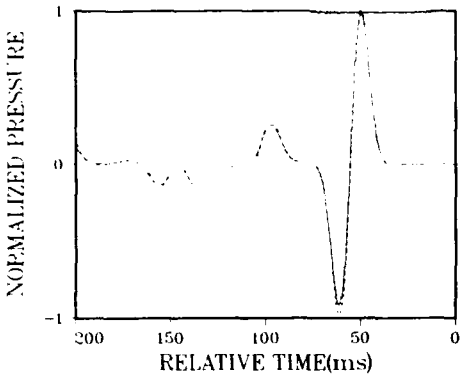

FIG. 4. TDPE solutions at $r = 500$ m and $z = 50$ m generated with the Gaussian starter (solid) and the half-space starter (dashed). The Gaussian-generated solution breaks down for late arrivals that propagate at large angles.

V. EFFICIENT PE AND RAY-TRACING CALCULATIONS

The PE method is valid for high frequencies. However, the computation time required for the numerical solution of the PE is proportional to the frequency squared in two dimensions. To avoid time-consuming calculations, one is tempted to apply ray theory. However, the ray theory solution can be unpleasant to implement due to the fact that it is implicit. In this section, we discuss approaches for speeding up PE calculations and for obtaining qualitative results efficiently with ray tracing.

One of the standard methods for matching the inner and outer solutions is to obtain the behavior of the inner solution in the outer region.[14] The half-space field P_h exhibits beams in the outer region due to the Lloyd's mirror effect. Thus one would expect the outer solution to consist of beams that are curved due to refraction. We illustrate the beams in the outer region for a 200-Hz source placed at $z_0 = 50$ m in a deep-water ocean with Munk's exponential sound-speed profile[15]

$$c_w(z) = c_{\rm ch}\left\{1 + \mu\left[2\frac{z - z_{\rm ch}}{H} + \exp\left(-2\frac{z - z_{\rm ch}}{H}\right) - 1\right]\right\}, \tag{47}$$

where $\mu \ll 1$, $z_{\rm ch}$ is the channel depth, $c_{\rm ch}$ is the channel speed, and H is the channel thickness. A plot of c_w appears in Fig. 5. A plot of PE-generated transmission loss appears in Fig. 6 for $\mu = 0.0071$, $c_{\rm ch} = 1500$ m/s, $z_{\rm ch} = 1000$ m, and $H = 1200$ m. The curved beams, which can be traced to the Lloyd's mirror beams near the source, are the dominant feature. The beams evolve to a constant width in the two-dimensional vertical cross section, which is necessary since cylindrical spreading applies in the sound channel. The PE calculation took 2.5 h on a Digital VAX-8650 computer.

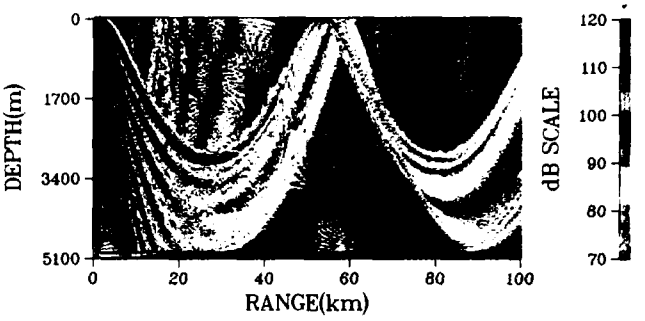

FIG. 6. PE-generated transmission loss. The curved beams of the outer solution can be traced back to the Lloyd's mirror beams near the origin.

The dipole behavior exhibited in Fig. 6 suggests an approach for speeding up PE calculations. Since the beam pattern is determined by $k_0 z_0$, transmission loss for the frequency ω can be approximated efficiently by replacing ω with $\zeta\omega$, z_0 with z_0/ζ, and β with β/ζ, where $\zeta < 1$. We refer to this approach as the ζ method. For it to be valid, $\zeta\omega$ must be large enough for ray theory to be valid. We illustrate the ζ method by taking $\zeta = 1/2$ for the 200-Hz problem with Munk's profile. The transmission loss plot obtained by the ζ method appears in Fig. 7 and agrees well with Fig. 6. Since the ζ method gives accurate results and decreases the run time by the factor ζ^2 in two dimensions and by the factor ζ^3 in three dimensions, it should be useful for underwater acoustics calculations.

Ray-tracing calculations are complicated because it is necessary to determine all of the rays that pass through a given point and sum their contributions to the field at that point. A simple way to avoid this difficulty is to take into account the behavior in the inner region. A good qualitative representation of the farfield is obtained by tracing rays from the origin in the directions of the Lloyd's mirror beams, as in Fig. 8. This calculation required just 3 s on a VAX-8650, yet the result gives a useful description of the farfield.

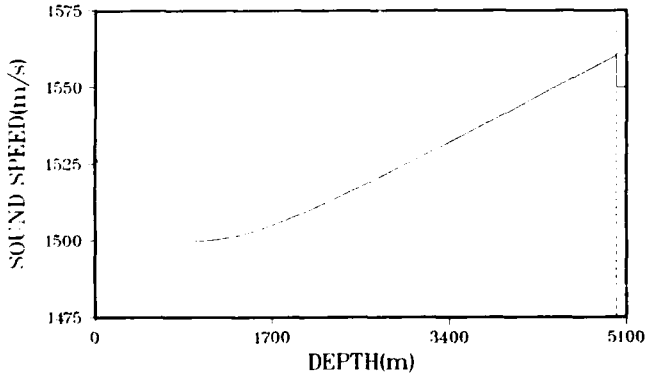

FIG. 5. Munk's deep-water sound-speed profile.

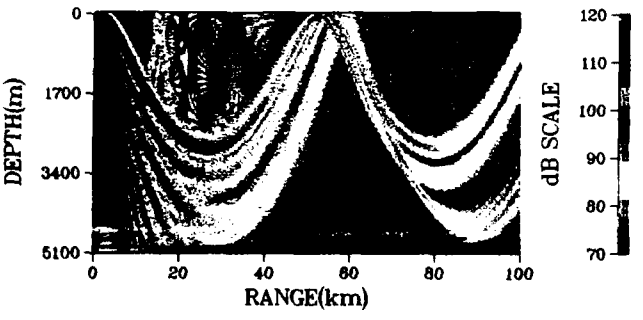

FIG. 7. The ζ method with $\zeta = 1/2$. There is good agreement with Fig. 6.

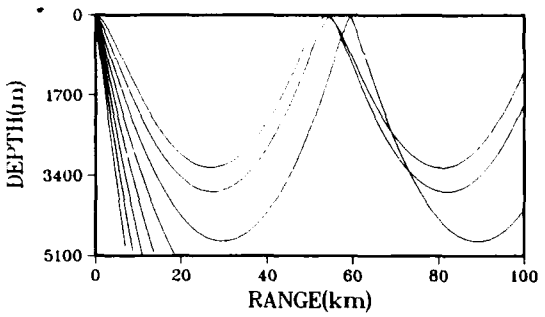

FIG. 8. Rays launched in the directions of the Lloyd's mirror beams to obtain the qualitative behavior in Fig. 6.

These concepts of ray-tracing and matched asymptotics combine to motivate an efficient method for source localization. Suppose that a high-frequency (> 100 Hz), time-harmonic signal from a point source of unknown location is received at a vertical array. Signal processing techniques can be used to determine the depths and angles of beam arrivals at the array. To determine the source location, rays corresponding to the beams are traced away from the array in both directions. The range of the source is the range at which all of the rays meet at one point on the ocean surface. The depth of the source is determined by the Lloyd's mirror beam pattern described by the rays at this range.

To further illustrate the ray-tracing method, we consider an ocean with the Munk profile used above and having the bathymetry

$$d(x,y) = d_0 - \sum_n h_n \exp(-\sigma_n^2), \tag{48}$$

$$\sigma_n^2 = [(x-x_n)^2 + (y-y_n)^2]/w_n^2 . \tag{49}$$

Data for this problem appear in Table IV. We apply the ray-tracing method to determine the locations at which beams are incident upon the ocean surface at the first two convergence zones and plot them in Fig. 9. Although beams lose energy as they reflect from the ocean bottom, they retain some energy, as is evident in the shadow zone for $z < 2500$ m and r near 25 km in Fig. 6. Thus we do not terminate the rays as they reflect from the seamounts. The seamounts result in various partial and total shadow zones. Some of the rays encounter the seamount nearest the origin two times producing additional cusps in the curves.

VI. CONCLUSIONS

The homogeneous half-space field is useful for time-harmonic and pulsed point and multipole sources in both two and three spatial dimensions. It is probably the simplest possible inner solution because it accounts for rays from both the source point and the image point at which a source of opposite phase is needed to account for the pressure release surface. The half-space field is easy to interpret physically. Refraction is weak in the ocean and can be neglected over short ranges. Reflections from the ocean bottom occur at large angles near the source and thus do not affect the far-field. These concepts lead to an important simplification of the scattering problem. The concepts of matched asymptotics motivate the ζ method and the ray-tracing model.

TABLE IV. Data for the three-dimensional ray-trace problem.

$x_1 = 20$ km	$x_2 = -70$ km	$x_3 = 10$ km
$y_1 = 0$	$y_2 = 20$ km	$y_3 = -60$ km
$h_1 = 2500$ m	$h_2 = 3000$ m	$h_3 = 2500$ m
$w_1 = 10$ km	$w_2 = 15$ km	$w_3 = 20$ km
$d_0 = 5000$ m	$\omega = 400\pi$ s^{-1}	$z_0 = 50$ m

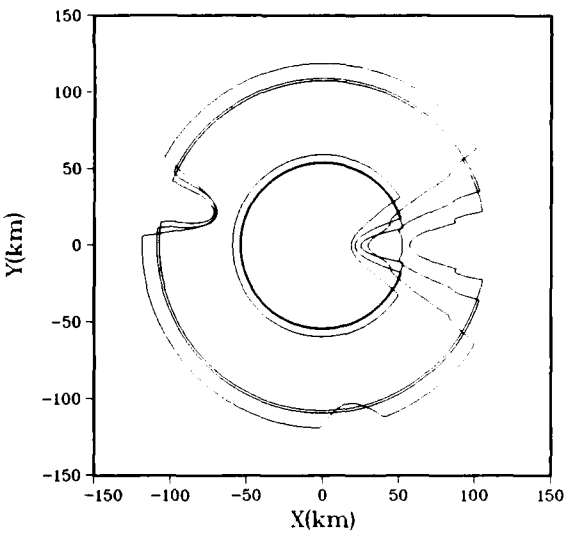

FIG. 9. View from above an ocean with seamounts. The curves mark the locations of beam arrivals at the ocean surface. Various shadow zones appear behind the seamounts.

ACKNOWLEDGMENTS

This work was supported by the Office of Naval Research and the Naval Ocean Research and Development Activity. The author thanks G. A. Kriegsmann and E. L. Reiss for supporting this work as part of a dissertation at Northwestern University.

APPENDIX: ASYMPTOTIC DERIVATION OF EIGENVALUES

We assume the following ansatz, which is similar to the WKBJ ansatz, for the eigenvalue problem:

$$P(r,z) \sim \pi i \sum_{n=1}^{N} \phi_n(z_0)\Phi_n(z)H_0^{(1)}(K_n r), \tag{A1}$$

$$\Phi_n(z) = \phi_n(z) + \psi_n(z) + \dots , \tag{A2}$$

$$K_n = k_n + i\gamma_n + \dots . \tag{A3}$$

Substituting the nth term of Eq. (A1) into Eq. (2), we obtain

$$L\psi_n - k_n^2\psi_n = 2i(-\sigma\beta k^2 + \gamma_n k_n)\phi_n . \tag{A4}$$

Equation (A4) has a solution only if the following solvability condition is satisfied:

$$\langle(-\sigma\beta k^2 + \gamma_n k_n)\phi_n, \phi_n\rangle = 0, \tag{A5}$$

$$\gamma_n = (\sigma/k_n)\langle\beta k^2, \phi_n^2\rangle . \tag{A6}$$

Equation (6) follows since $k \sim k_0$ and $k_n \sim k_0$.

[1] F. D. Tappert, "The Parabolic Approximation Method," in *Wave Propagation and Underwater Acoustics*, edited by J. B. Keller and J. S. Papadakis, Lecture Notes in Physics (Springer, New York, 1977), Vol. 70.

[3]"NORDA Parabolic Equation Workshop," edited by J. A. Davis, D. White, and R. C. Cavanagh, NORDA Tech. Note 143, 22–24 (1982).
[4]R. R. Green, "The Rational Approximation to the Acoustic Wave Equation with Bottom Interaction," J. Acoust. Soc. Am. **76**, 1764–1773 (1984).
[5]E. R. Robinson and D. H. Wood, "Generating Direct Starting Fields for Parabolic Equations," J. Acoust. Soc. Am. **84**, 1794–1801 (1988).
[6]C. M. Bender and S. A. Orszag, *Advanced Mathematical Methods for Scientists and Engineers* (McGraw-Hill, New York, 1978), pp. 417–483.
[7]N. Bleistein and R. A. Handelsman, *Asymptotic Expansions of Integrals* (Dover, New York, 1986), pp. 219–224.
[8]A. D. Pierce, "Augmented Adiabatic Mode Theory for Upslope Propagation from a Point Source in Variable-Depth Shallow Water Overlying a Fluid Bottom," J. Acoust. Soc. Am. **74**, 1837–1847 (1983).
[9]P. G. Bergmann, "The Wave Equation in a Medium with a Variable Index of Refraction," J. Acoust. Soc. Am. **17**, 329–333 (1946).
[10]M. D. Collins, "The Time-Domain Solution of the Wide-Angle Parabolic Equation Including the Effects of Sediment Dispersion," J. Acoust. Soc. Am. **84**, 2114–2125 (1988).
[11]M. D. Collins, "Low-Frequency, Bottom-Interacting Pulse Propagation in the Ocean," IEEE J. Ocean Eng. **13-4**, 222–228 (1988).
[12]R. H. Hackman and G. S. Sammelmann, "Acoustic Scattering in an Inhomogeneous Waveguide: Theory," J. Acoust. Soc. Am. **80**, 1447–1458 (1986).
[13]F. Ingenito, "Scattering from an Object in a Stratified Medium," J. Acoust. Soc. Am. **82**, 2051–2059 (1987).
[14]M. D. Collins and M. F. Werby, "A Parabolic Equation Model for Scattering in the Ocean," J. Acoust. Soc. Am. (accepted for publication).
[15]A. H. Nayfeh, *Introduction to Perturbation Techniques* (Wiley, New York, 1981), pp. 265–268.
[16]W. H. Munk, "Sound Channel in an Exponentially Stratified Ocean with Applications to SOFAR," J. Acoust. Soc. Am. **55**, 220–226 (1974).